

# FlexDiT: Dynamic Token Density Control for Diffusion Transformer

Shuning Chang<sup>1,2</sup> Pichao Wang Jiasheng Tang<sup>2</sup> Yi Yang<sup>1</sup>

<sup>1</sup>Zhejiang University <sup>2</sup>Alibaba Group

{shuning.csn, jiasheng.tjs}@alibaba-inc.com, pichaowang@gmail.com, yangyics@zju.edu

## Abstract

*Diffusion Transformers (DiT) deliver impressive generative performance but face prohibitive computational demands due to both the quadratic complexity of token-based self-attention and the need for extensive sampling steps. While recent research has focused on accelerating sampling, the structural inefficiencies of DiT remain underexplored. We propose **FlexDiT**, a framework that dynamically adapts token density across both spatial and temporal dimensions to achieve computational efficiency without compromising generation quality. Spatially, FlexDiT employs a three-segment architecture that allocates token density based on feature requirements at each layer: Poolingformer in the bottom layers for efficient global feature extraction, Sparse-Dense Token Modules (SDTM) in the middle layers to balance global context with local detail, and dense tokens in the top layers to refine high-frequency details. Temporally, FlexDiT dynamically modulates token density across denoising stages, progressively increasing token count as finer details emerge in later timesteps. This synergy between FlexDiT’s spatially adaptive architecture and its temporal pruning strategy enables a unified framework that balances efficiency and fidelity throughout the generation process. Our experiments demonstrate FlexDiT’s effectiveness, achieving a 55% reduction in FLOPs and a 175% improvement in inference speed on DiT-XL with only a 0.09 increase in FID score on  $512 \times 512$  ImageNet images, a 56% reduction in FLOPs across video generation datasets including FaceForensics, SkyTimelapse, UCF101, and Taichi-HD, and a 69% improvement in inference speed on PixArt- $\alpha$  on text-to-image generation task with a 0.24 FID score decrease. FlexDiT provides a scalable solution for high-quality diffusion-based generation compatible with further sampling optimization techniques. Code will be available at <https://github.com/changsn/FlexDiT>.*

## 1. Introduction

Diffusion models [3, 12, 19, 43] have emerged as powerful tools in visual generation, producing photorealistic images

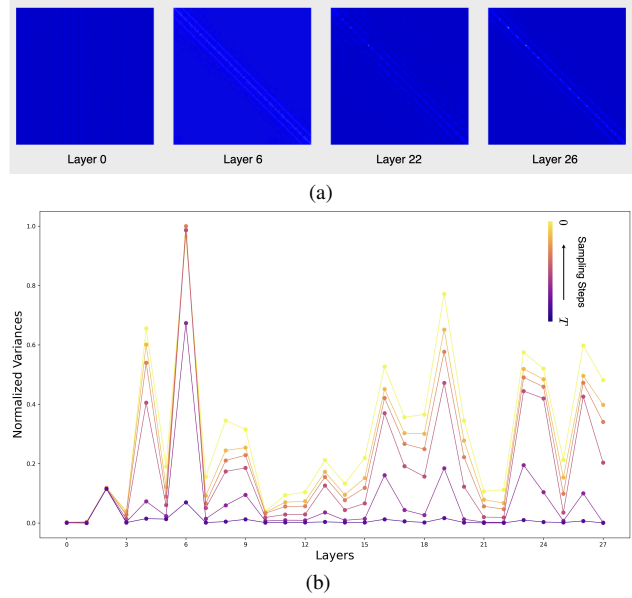


Figure 1. (a) The attention maps in different self-attention layers. Zoom-in for better visibility. (b) The normalized variances of attention maps in DiT-XL. Different curve lines represent different sampling steps.

and videos by gradually refining structured content from noise. Leveraging the scalability of Transformers, Diffusion Transformer (DiT) models [2, 40] extend these capabilities to more complex and detailed tasks [13, 62] and form the backbone of advanced generation frameworks such as Sora [6]. Yet, despite their impressive generative capabilities, DiT models face significant computational limitations that restrict their broader applicability, especially in scenarios where efficiency is paramount.

The computational burden of DiT models arises mainly from the need for numerous sampling steps in the denoising process and the quadratic complexity of Transformer structures with respect to the number of tokens. Although recent research has focused on reducing this burden by accelerating the sampling process through techniques such as ODE solvers [29, 51], flow-based methods [26, 28], and knowledge distillation [31, 34, 46, 53, 63], these approaches often overlook the core architectural inefficiencies

of DiT itself. Unlike U-Net-based architectures [44], which mitigate complexity through a contracting-expansive structure, DiT’s reliance on token-level self-attention incurs high costs that scale with model size and token count. This bottleneck highlights a critical need for DiT-specific innovations that manage token density intelligently, balancing efficiency and quality without sacrificing generation fidelity.

To address this challenge, we examine the distribution of attention across DiT’s layers and sampling steps, seeking to uncover structural patterns that could guide more efficient token management. As illustrated in Figure 1a, attention maps reveal that tokens capture different levels of granularity across layers: in the bottom layers, such as layer 0, attention maps appear uniformly distributed, indicating a focus on broad, global features akin to global pooling. Meanwhile, middle layers alternate in their attention, with certain layers (e.g., layer 6 and layer 26) capturing local details, while others (e.g., layer 22) emphasize global structure. This observation is quantified in Figure 1b, where the variance in attention scores highlights DiT’s consistent pattern of alternation between global and local feature extraction across layers. In addition to spatial analysis, Figure 1b also reveals insights across sampling steps. We observe that, while the pattern of alternation between global and local focus remains stable, attention variance increases as the denoising process advances, indicating a growing emphasis on local information at lower-noise stages. This analysis yields three core insights: (1) the initial self-attention layers exhibit minimal variance, showing low discrepancy in feature extraction across tokens; (2) DiT’s architecture inherently alternates between global and local feature focus across layers, a pattern consistent across all sampling steps; and (3) as denoising progresses, the model increasingly prioritizes local details, dynamically adapting to heightened demands for detail at later stages.

Building on these insights, we propose FlexDiT, which reimagines token density management as a dynamic process adapting across both spatial layers and temporal stages. Spatially, shallow layers capture smooth, global features, making complex self-attention less efficient. Subsequent layers alternate between high-frequency local details and low-frequency global information, where sparse tokens efficiently capture global features, and dense tokens refine local details. Temporally, as denoising advances, the need for local detail increases, motivating a dynamic token adjustment strategy. This dual-layered adaptation integrates layer-wise token modulation—balancing efficiency and detail within each sampling step—and a timestep-wise pruning strategy that adjusts token density dynamically. Together, these spatial and temporal adaptations allow FlexDiT to achieve computational efficiency without sacrificing high-fidelity detail, as reflected in FlexDiT’s architectural design and pruning strategy, tailored to meet the unique spatial and

temporal demands of the generation process.

**FlexDiT Architecture:** FlexDiT’s architecture employs a three-segment design that aligns token density with the features each layer captures. In the bottom layers, we replace self-attention with a poolingformer structure to capture broad global features through average pooling, reducing computation while preserving essential structure. In the middle layers, FlexDiT introduces Sparse-Dense Token Modules (SDTM), blending sparse tokens for global structure with dense tokens to refine local details. This design enables FlexDiT to retain efficiency while maintaining stability and detail. In the top layers, the model processes all tokens densely, focusing on high-frequency details for refined output quality.

**Timestep-Wise Pruning Rate Strategy:** Complementing spatial adjustments, FlexDiT’s timestep-wise pruning rate strategy adapts token density across denoising stages. In early stages, where broad, low-frequency structures dominate, FlexDiT applies a high pruning rate, conserving resources. As the process progresses and intricate details emerge, the pruning rate decreases, allowing for a gradual increase in token density. This adjustment aligns computational effort with each stage’s complexity, dynamically balancing efficiency and detail to optimize resources for high-fidelity output.

Our empirical results substantiate the effectiveness of FlexDiT’s integrated approach. FlexDiT reduces the FLOPs of DiT-XL by 55% and improves inference speed by 175% on  $512 \times 512$  ImageNet [11] images, with only a 0.09 increase in FID score [17]. On the Latte-XL dataset [33], FlexDiT achieves a 56% reduction in FLOPs across standard video generation datasets, including FaceForensics [45], SkyTimelapse [60], UCF101 [54], and Taichi-HD [50]. Additionally, on the more challenging text-to-image generation task, we achieve a 69% improvement in inference speed on PixArt- $\alpha$  with a 0.24 FID score reduction. These results demonstrate FlexDiT’s capability to provide an efficient, high-quality architecture for diffusion-based generation, compatible with further sampling optimization techniques for enhanced efficiency.

## 2. Related works

Although diffusion models [19, 43] have achieved impressive performance in generation tasks, their generation speed remains a significant bottleneck for broader applications. This limitation arises primarily from the step-wise reverse diffusion process and the high computational cost associated with single model evaluations.

**Efficient sampling process.** This direction focuses on optimizing sampling steps in diffusion models. Some approaches [1, 29, 30, 51] design new solvers to achieve faster sampling with fewer steps. Consistency models

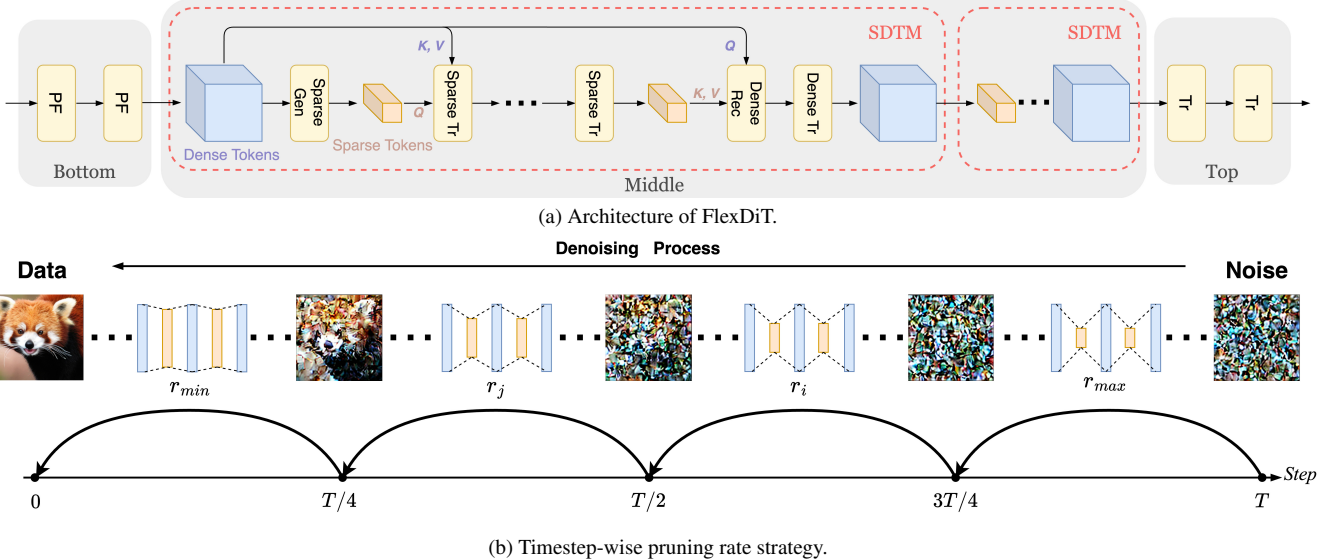


Figure 2. Architecture of FlexDiT and timestep-wise pruning rate strategy. The architecture consists of three segments: bottom, middle, and top. The bottom segment includes poolingformers (PF). The middle segment comprises multiple sparse-dense token modules (SDTMs), where sparse token generation transformers (“Sparse Gen”) and dense token recovery transformers (“Dense Rec”) alternate to balance global and detailed information processing. The top segment contains standard transformers (“Tr”) for final processing. During the denoising process, we apply varying pruning rates  $r$  at different stages (depicted as four stages).

(CMs) [21, 31, 52, 53, 58] are closely related to diffusion models, achieving by distilling pre-trained diffusion models or training from scratch. These models learn a one-step mapping between noise and data, and all the points of the sampling trajectory map to the same initial data point. Flow-based [13, 26, 28, 67, 68] approaches straighten the transport trajectories among different distributions and thereby realize efficient inference. Knowledge distillation are applied by some methods [31, 34, 46, 53, 63] to reduce the sampling steps and match the output of the combined conditional and unconditional models. Parallel sampling techniques [49, 56, 66] employ Picard-Lindelöf iteration or Fourier neural operators for solving SDE/ODE.

**Efficient model structure.** Another avenue focuses on improving inference time within a single model evaluation. Some methods attempt to compress the size of diffusion models via pruning [14] or quantization [25, 48]. Spectral Diffusion [61] boosts structure design by incorporating frequency dynamics and priors. OMS-DPM [27] proposes a model schedule that selects small models or large models at specific sampling steps to balance generation quality and inference speed. Deepcache [32] reuse or share similar features across sampling steps. The early stopping mechanism in diffusion is explored in [24, 36, 55].

Most of the above methods are designed for general diffusion models. Recently, the Diffusion Transformer (DiT) has emerged as a more potential backbone, surpassing the previously dominant U-Net architectures. Un-

like U-Net-based models, DiT’s inefficiency stems largely from the self-attention mechanism. Limited research has specifically addressed the efficiency of DiT-based models. [42] identifies the redundancies in the self-attention and adopts timestep dynamic mediator tokens to compress attention complexity, achieving some performances but limited FLOPs reduction, as this approach primarily reduces the number of keys and values rather than the overall tokens count. In Vision transformers for classification task, numerous methods [5, 7, 9, 15, 35, 59, 69] successfully removed redundant tokens to improve performance-efficiency trade-offs. ToMeSD [4] is the first to explore token reduction in diffusion models. However, its performance on DiT was suboptimal, as shown in [36, 65]. U-Net can be regarded as a sparse network due to its contracting and expansive structure. EDT [10] applies a novel architecture similar to U-Net, while they still have 1.4 FID score gap compared to its baseline model MDTv2 [16] via 2,000K iterations. These findings indicate that directly transferring token reduction techniques from classification tasks or reusing U-Net structures may be insufficient for DiT. Instead, a specialized token reduction strategy is needed.

We analyze the structure of DiT and observe that local and global features are captured alternately across layers. Inspired by this insight, FlexDiT introduces a novel token reduction strategy that decouples the generation process into separate integration of global and local information, leveraging sparse tokens for global feature extraction and dense tokens for local detail refinement. By alternat-

ing between sparse and dense tokens, FlexDiT ensures high efficiency and performance.

### 3. Method

We first provide an overview of diffusion models and DiT in Section 3.1. FlexDiT architecture is then introduced in Section 3.2, followed by our timestep-wise pruning rate strategy in Section 3.3. Finally, Section 3.4 details the initialization and fine-tuning of our network.

#### 3.1. Preliminary

**Diffusion models** generate visual contents (such as images and videos) from random noise through a series of denoising steps. These models typically consist of a forward diffusion process and a reverse denoising process. In the forward process, given a visual input  $x_0 \sim q(x)$  sampled from the data distribution, Gaussian noise  $\epsilon \sim \mathcal{N}(0, I)$  is progressively added over  $T$  steps. This process is defined as  $q(x_t|x_{t-1}) = \mathcal{N}(x_t; \sqrt{1 - \beta_t}x_{t-1}, \beta_t I)$ , where  $t$  and  $\beta_t$  denote the sampling step and noise schedule, separately. In the reverse process, the model removes the noise and reconstructs  $x_0$  from  $x_T \sim \mathcal{N}(0, I)$  using  $p_\theta(x_{t-1}|x_t) = \mathcal{N}(x_{t-1}; \mu_\theta(x_t, t), \sum_\theta(x_t, t))$ , where  $\mu_\theta(x_t, t)$  and  $\sum_\theta(x_t, t)$  represent the mean and variance of the Gaussian distribution.

**Diffusion transformer (DiT)** exhibits the scalability and promising performance of transformers. Similar to ViT, DiT consists of layers composed of a multi-head self-attention (MHSA) layer and a multi-layer perceptron (MLP) layer, described as

$$\begin{aligned} X &= X + \alpha M H S A(\gamma X + \beta), \\ X &= X + \alpha' M L P(\gamma' X + \beta'), \end{aligned} \quad (1)$$

where  $X \in \mathbb{R}^{N \times C}$  denotes input tokens,  $N$  is the number of tokens, and  $C$  is the channel dimension. The parameters  $\{\alpha, \gamma, \beta, \alpha', \gamma', \beta'\}$  are produced by an adaptive layer norm (AdaLN) block [41], which takes the condition embedding and sampling step embedding as inputs.

#### 3.2. FlexDiT

**Overview architecture.** The FlexDiT architecture is illustrated in Figure 2a, where the transformer layers of DiT based model are divided into three groups: bottom, middle, and top. The bottom layers leverage poolingformers to efficiently capture global features. The middle layers contain multiple sparse-dense token modules (SDTM), which decouple the representation process into global structure capture and local details enhancement using sparse and dense tokens, respectively. The top layers retain the standard transformers, processing dense tokens to generate the



(a) Standard DiT-XL.



(b) Replacing the first two attention maps in DiT-XL with full-one matrices without fine-tuning.

Figure 3. Comparison of images generated by the standard DiT-XL model and a modified DiT-XL model where the first two attention maps are replaced with full-one matrices. Both sets of images exhibit similar visual quality.

final predictions at each sampling step. The primary computational savings are achieved through sparse tokens, hence the majority of transformer layers are located in the middle section to maximize efficiency.

**Poolingformer in the bottom layers.** As shown in the first subfigure in Figure 1a, attention scores in the bottom layers are uniformly distributed, with each token evenly extracting global features, akin to a global average pooling operator. To investigate further, we conducted a toy experiment where the attention maps in the first two transformer layers were replaced with matrices filled with 1, without any fine-tuning. Figure 3 shows that, using the same initial noise and random seed, the images generated by both the original DiT-XL and the modified DiT-XL are nearly identical, suggesting that complex self-attention calculations offer limited additional information. Given that self-attention in the bottom layers captures global features, we question whether sparse tokens can be used in these layers. Extensive experiments, however, demonstrated that applying sparse tokens in the lower layers leads to unstable training; maintaining a full set of tokens in these layers is essential.

Based on above analysis, we adopt poolingformers to replace the original transformers. In poolingformer, we re-

move the queries and keys as attention maps are not computed. Instead, we perform global pooling on the value  $V \in \mathbb{R}^{N \times C}$  and integrate it into input tokens  $X$ , which can be represented as

$$X = X + \bar{V}, \quad (2)$$

where  $\bar{V}$  is the mean along the dimension of  $N$ , *i.e.*,  $\bar{v} = \frac{1}{N} \sum V(\bar{v} \in \mathbb{R}^{1 \times C})$ , and then repeating  $N$  times to shape  $N \times C$ . The parameters from adaLN block are omitted in all the equations for brevity. Our poolingformer can be viewed as a special case of the model in [64], behaving identically when the average pooling kernel size equals the input size.

**Sparse-dense token module.** We present the sparse-dense token module (SDTM) to generate sparse and dense tokens processed by corresponding transformer layers. The high-level idea is to decouple global structure extraction and local detail extraction. Sparse tokens capture global structure information and reduce computational cost, while dense tokens enhance local detail and stabilize training. Sparse and dense tokens are converted each other within SDTM.

Initially, SDTM introduces a set of sparse tokens  $X_s \in \mathbb{R}^{M \times C}$ , where  $M$  is the number of sparse tokens, typically  $M \ll N$ . We define pruning rate  $r = 1 - M/N$  to represent the sparsity degree. Sparse token interact with full-size dense tokens via an attention layer to integrate the global information:

$$X_s = X_s + MHA(X_s, X, X), \quad (3)$$

where the triplet input of  $MHA$  are queries, keys, and values in turn. Sparse tokens can be initialized by adaptively pooling the dense tokens  $X$ . To store the structure information, we first reshape the dense tokens  $X \in \mathbb{R}^{N \times C}$  into the latent shape. For instance, if the input is an image, we reshape it into shape  $H \times W \times C$ , then pool it across the spatial dimensions to shape  $H' \times W' \times C$ , where  $M = H' \times W'$  and  $r = 1 - (H' \cdot W')/(H \cdot W)$ . The intentions of spatial pooling initialization are two folds. First, the initial sparse tokens can distribute uniformly in space and the representation of each sparse tokens is associated with a specific spatial location, beneficial for downstream tasks like image editing [20]. Second, it can prevent the semantic tokens from collapsing to one point in the following layers.

The generated sparse tokens are fed into subsequent transformer layers, referred to as sparse transformers. Since  $M \ll N$ , our SDTM can substantially reduce the computational cost.

At the rear of SDTM, we restore dense tokens from sparse tokens. First, we reshape the sparse tokens  $X_s \in \mathbb{R}^{M \times C}$  into structure shape  $H' \times W' \times C$  and upsample it to the same shape as input dense tokens  $X \in \mathbb{R}^{H \times W \times C}$ . We

introduce two linear layers to combine upsampling sparse tokens with dense tokens, which is represented as:

$$X_{merged} = UpSample(X_s) \cdot W_1 + X \cdot W_2, \quad (4)$$

where  $W_1, W_2 \in \mathbb{R}^{C \times C}$  are the weights of two linear layers. Then, to further incorporate sparse tokens, we utilize an attention layer to perform a reverse operation of the generation of sparse token to produce the restored dense tokens, which is written as:

$$X = X_{merged} + MHA(X_{merged}, X_s, X_s). \quad (5)$$

At the end of SDTM, several transformer layers, referred as to dense transformers process full-size dense tokens to enhance local details.

We cascade multiple SDTMs in our network. By repeating sparse and dense tokens, the network effectively preserves both structural and detailed information, achieving substantial reductions in computational cost while maintaining high-quality generation outputs.

### 3.3. Timestep-wise pruning rate.

We have observed that the tokens display varying denoising behavior over sampling steps. They generate the low-frequency global structure information in the early denoising stage and the high frequency details in the late denoising stage. The token count requirement is progressively increase along sampling steps. We exploit this by dynamically adjusting the pruning rate  $r$  across sampling steps, increasing tokens as sampling progresses.

Given  $T$  sampling steps, we propose a sample-specific approach to dynamically adjust the pruning rate  $r$ , thereby controlling the number of sparse tokens across sampling steps. We define a range for  $r$ , such that  $r \in [r_{min}, r_{max}]$ . Observing that generation quality is highly relative with the later denoising stages (in Section 4.4), we hold  $r$  constant at  $r_{min}$  for the first  $T/4$  sampling steps. Subsequently, we adjust the pruning rate  $r$  linearly based on the current sampling step  $t_i$ . The specific formula for  $r$  is provided as follows:

$$r = \begin{cases} r_{min}, & t_i < T/4, \\ \frac{4T-4}{3T} r_{min} + \frac{4-T}{3T} r_{max}, & T/4 \leq t_i < T. \end{cases} \quad (6)$$

During training, we sample step  $t_i$  and compute the corresponding  $r$  according to Eq. 6. However, the tokens of input should be same to train the model in batch, and the randomness of sampling from  $T$  also need to be maintained. To solve this contradiction, we modify the linear function of Eq. 6 when  $T/4 \leq t_i < T$  to piecewise function. Normally, the model is trained by multiple GPUs. We request the  $t_i$  sampled in a specific piece in each GPU. Therefore, in each iteration, it can achieve both uniformly random sampling and training in batch.

Resolution	Model	FLOPs (G)	Throughput (img/s)	FID ↓	sFID ↓	IS ↑	Precision ↑	Recall ↑
256 × 256	DiT-B	23.01	7.84	9.07	5.44	121.07	0.74	0.54
	<b>Ours</b> ( $r \in [0.61, 0.86]$ )	14.34 (-38%)	13.2 (+68%)	8.23	6.20	134.30	0.74	0.54
256 × 256	DiT-XL	118.64	1.58	2.27	4.60	278.24	0.83	0.57
	<b>Ours</b> ( $r \in [0.61, 0.44]$ )	88.91 (-25%)	2.13 (+35%)	2.23	4.62	278.91	0.84	0.58
	<b>Ours</b> ( $r \in [0.61, 0.86]$ )	68.05 (-43%)	2.95 (+87%)	2.38	4.82	276.39	0.82	0.58
512 × 512	DiT-XL	525	0.249	3.04	5.02	240.82	0.84	0.54
	<b>Ours</b> ( $r \in [0.61, 0.86]$ )	286 (-46%)	0.609 (+145%)	2.96	5.00	242.4	0.84	0.54
	<b>Ours</b> ( $r \in [0.90, 0.96]$ )	235 (-55%)	0.685 (+175%)	3.13	5.41	236.56	0.83	0.52

Table 1. Comparison of performance between FlexDiT and DiT for class-conditional image generation task on ImageNet.

### 3.4. Initialization and fine-tuning.

Our method fine-tunes pre-trained DiT models to improve efficiency. The processes of generating sparse tokens and restoring dense tokens utilize off-the-shelf transformers, avoiding the need for additional networks. During fine-tuning, the parameters of transformers in DiT-based model are loaded into the corresponding transformers in our FlexDiT, with two exceptions: (1) queries and keys are absent in Poolingformers, hence related parameters in pre-trained model are not required; (2) the weights  $W_1$  and  $W_2$  in Eq. 4 are initialized by full zeros and identity matrix, respectively.

## 4. Experiments

FlexDiT is applied in three representative DiT-based models, DiT [40], Latte [33], and PixArt- $\alpha$  [8] for class-conditional image generation and video generation, and text-to-image generation, respectively.

### 4.1. Class-conditional image generation

**Experimental setting.** We conduct our experiments on ImageNet-1k [11] at resolutions of  $256 \times 256$  and  $512 \times 512$ , following the protocol established in DiT. For DiT-XL, the model consists of 2, 24, and 2 transformer layers in the bottom, middle, and top segments, respectively. The middle segment includes 4 sparse-dense token modules, which comprise 1 sparse token generation transformer, 3 sparse transformers, 1 dense token recovery transformer, and 1 dense transformer. For DiT-B, the bottom, middle, and top segments contain 1, 10, and 1 transformer layers, respectively. The middle segment consists of 2 sparse-dense token modules, including 1 sparse token generation transformer, 2 sparse transformers, 1 dense token recovery transformer, and 1 dense transformer.

As poolingformers and sparse transformers can interfere with the function of position embedding, we reintroduce sine-cosine position embedding at each stage of dense token generation. For DiT-XL, we use the checkpoint from the official DiT repository, while for DiT-B, we utilize the

checkpoint provided by [39]. All training settings and hyperparameters follow those in the original DiT paper. The strength of classifier-free guidance [18] is set to 1.5 for evaluation and 4.0 for visualization.

Following prior works, we sample 50,000 images to compute the Fréchet Inception Distance (FID) [17] using the ADM TensorFlow evaluation suite [12], along with the Inception Score (IS) [47], sFID [37], and Precision-Recall metrics [23]. Throughput is evaluated with a batch size of 128 on an Nvidia A100 GPU.

**Main results.** The results of our approach on the class-conditional image generation task using ImageNet are presented in Table 1. We evaluate our method on two model sizes, DiT-B and DiT-XL, and at two resolutions,  $256 \times 256$  and  $512 \times 512$ . At pruning rates  $r \in [0.61, 0.86]$ , FlexDiT-XL achieves a 43% reduction in FLOPs and an 87% improvement in inference speed, with only a 0.11 increase in FID score. This indicates significant redundancy within DiT, as using only about 25% tokens in specific layers maintains similar performance levels. By increasing the token count, we observe slight improvements over baseline performance with 145% improvement in throughput. The impact of our approach is even more pronounced at a resolution of  $512 \times 512$ . With a higher pruning rate than the  $256 \times 256$  resolution, our method yields a superior performance-efficiency trade-off. By pruning over 90% of the tokens, we achieve a 55% reduction in FLOPs and a 175% increase in throughput, with only a 0.09 increase in FID score. When reducing the pruning rate further, our results slightly surpass the baseline, delivering a 145% throughput improvement.

From  $256 \times 256$  to  $512 \times 512$ , the FLOPs increase by only 4.4 times, whereas the speed declines by a factor of 6.3, demonstrating that the primary speed bottleneck in DiT structure is the number of tokens. Our method effectively reduces token count, resulting in significant gains, particularly for high-resolution content generation. For instance, we achieve a 55% reduction in FLOPs at  $512 \times 512$  while enhancing speed by 175%. Compared to other methods, our



(a) Images generated by DiT.

(b) Images generated by FlexDiT (-43% FLOPs).

Figure 4. Generating images from DiT-XL and FlexDiT-XL with the same random seed.

Model	FLOPs (G)	Throughput (clip/s)	FaceForensic	SkyTimelapse	UCF101	Taichi-HD
Latte-XL*	1894	0.108	24.10	40.78	284.54	89.63
<b>Ours (<math>r \in [0.80, 0.93]</math>)</b>	828 (-56%)	0.228 (+111%)	24.51	39.02	288.90	84.13

Table 2. FVD scores of FlexDiT-XL in class-conditional video generation task on four mainstream video generation datasets. We do not find the official reference sets of these 4 dataset when we compute FVD scores, hence we build the reference sets by ourselves and use the official checkpoint to re-compute the FVD scores of Latte-XL in this table.

real-world speed improvements far exceed those achieved with similar reductions in FLOPs.

**Visualization results.** To further validate the effectiveness of our method, we visualize some samples generated from FlexDiT-XL at a  $256 \times 256$  resolution with a pruning rate  $r \in [0.61, 0.86]$  (-43% FLOPs) and compare them with DiT-XL in Figure 4. Each cell in the same position corresponds to images generated from the same random seed and class. Since our model is fine-tuned from the pre-trained DiT, the overall styles and structures of the two subfigures are similar. The images generated by FlexDiT still retain rich high-frequency details. Furthermore, FlexDiT images demonstrate more precise structure, as evidenced by the accurate depiction of the “golden retriever’s” nose and the “macaw’s” eyes, which appear misplacement or missing in the images generated by DiT-XL. We provide samples at a resolution of  $512 \times 512$  in Supplementary [?].

## 4.2. Class-conditional video generation

**Experimental settings.** We conduct experiments at a resolution of  $256 \times 256$  on four public datasets: FaceForensics [45], SkyTimelapse [60], UCF101 [54], and Taichi-HD [50]. Latte comprises two distinct types of transformer blocks: spatial transformers, which focus on capturing spatial information, and temporal transformers, which capture temporal information. To accommodate this separation of spatial and temporal feature extraction, we adjust our model’s schedule within the sparse-dense token module. Specifically, we employ two transformers to prune spatial tokens and temporal tokens separately. The sparse tokens are then processed by two sparse transformers, and finally,

two transformers are used to recover the temporal and spatial tokens. Dense transformers are discarded in this setup. All other model configurations are the same as in DiT, and we follow the original training settings and hyperparameters used for Latte.

To evaluate performance, we sample 2,048 videos, each consisting of 16 frames, and measure the Fréchet Video Distance (FVD) [57]. Throughput is measured using a batch size of 2 clips on an Nvidia A100 GPU.

**Main results.** Table 2 presents the main results of our approach. Leveraging the additional temporal dimension in video data allows for a higher pruning rate. Our method achieves a 56% reduction in FLOPs while maintaining a competitive FVD score compared to the baseline, demonstrating its effectiveness in video generation tasks.

## 4.3. Text-to-image generation

**Experiment setting** We further assess the effectiveness of our method on text-to-image generation, which presents a greater challenge compared to class-conditional image generation. We adopt PixArt- $\alpha$  [8], a text-to-image generation model built based on DiT as the base model. Our model is initialized using the official PixArt- $\alpha$  checkpoint pre-trained on SAM dataset [22] containing 10M images. We further fine-tune it with our method on a subset of SAM dataset including 1M images. In PixArt- $\alpha$ , the transformer architecture includes two types of attention layers: a self-attention layer and a cross-attention layer, which integrates textual information. We apply our method to the self-attention layers to either reduce or recover tokens.

Model	FLOPs (G)	Throughput(img/s)	FID ↓
PixArt- $\alpha$	148.73	0.414	4.53
Ours	91.62 (-38%)	0.701 (+69%)	4.29

Table 3. Text-to-image generation on SAM dataset.  $r \in [0.61, 0.86]$ .



Figure 5. Generating images from PixArt- $\alpha$  (a) and FlexDiT (b). The captions in the same positions are same. The captions are presented in Supplementary 7.

For evaluation, we randomly select text prompts from SAM dataset and adopt 100-step IDDPMP solver [38] to sample 30,000 images, with the FID score serving as the evaluation metric. Throughput is evaluated with a batch size of 128 on an Nvidia A100 GPU.

**Main results** As shown in Table 3, our FlexDiT achieves an FID score comparable to the original PixArt- $\alpha$  with significantly accelerating the generation, showing that our method is effective for text-to-image generation task and shows a strong general-purpose ability in various generation fields.

**Visualization results.** We visualize some samples of our method and compare them with original PixArt- $\alpha$  in Figure 5. The classifier-free guidance is set to 4.5. The results demonstrate that our method effectively maintains both image quality and semantic fidelity.

#### 4.4. Ablation study

All the following ablation experiments of FlexDiT-XL are conducted on ImageNet at a  $256 \times 256$  resolution.

**The number of SDTMs.** The alternation between sparse and dense tokens is a key factor contributing to the success of our method. Sparse tokens efficiently capture global structures, while dense tokens capture detailed information. In FlexDiT, we adopt four SDTMs by default. Table 4

No. of SDTMs	1	2	3	4
FID ↓	NAN	3.86	2.51	2.38
FLOPs	68.74	67.00	69.97	68.05

Table 4. Performance evaluation on different numbers of SDTMs. “NAN” indicates loss nan during training.

No. of Poolingformers	0	1	2	3
No. of trans in top seg.	4	3	2	1
FID ↓	NAN	2.38	2.38	2.56
FLOPs	69.56	68.80	68.05	67.29

Table 5. Performance evaluation on different numbers of pooling-formers. “NAN” indicates loss nan during training.

Model	250-DDPM	25-DDIM	5-RFlow
DiT-XL	2.27	2.89	43.40
Ours	2.38	3.31	43.69

Table 6. Combination our method with efficient samplers. The numbers represent FID scores.

FLOPs (G)	No. of Tokens	Dynamic	FID ↓
$\sim 68$	$8 \times 8$	✓	2.48
	$6 \times 6 \sim 10 \times 10$		2.38
$\sim 61$	$6 \times 6$	✓	2.63
	$4 \times 4 \sim 8 \times 8$		2.50

Table 7. Comparison of FID scores with and without timestep-wise pruning rate strategy.

shows the effect of using different numbers of SDTMs. To isolate the impact of SDTM count, we maintain the same FLOPs across models by adjusting the number of sparse and dense transformers while varying only the number of SDTMs. In configurations with only one SDTM, the model is modified into a U-shaped architecture, allocating 6 transformers to the bottom segment, 16 to a single SDTM, and 6 to the top segment. Note that in this configuration, standard transformers are used in the bottom layers instead of poolingformers prevent any performance degradation that arises from the use of poolingformers. The results indicate that fewer SDTMs reduce interactions between global and local information, resulting in weaker performance. Furthermore, when FlexDiT is reduced to a U-Net structure, training stability is compromised, resulting in training collapse. We do not experiment with more than four SDTMs, as increasing SDTM count beyond four offers diminishing returns in FLOP reduction. Using four SDTMs achieves an optimal balance between performance and efficiency.

**The number of poolingformers.** In Table 5, we examine the impact of varying the number of poolingformers in the model. We keep the total number of transformers in the bottom and top segments constant across configurations. When using three poolingformers, performance declines substantially due to the global average pooling operator’s limited ability to adaptively capture information. For configurations with one or two poolingformers, the models achieve same results. The poolingformer is more efficient and consume fewer parameters than the standard transformer; therefore, we default to using 2 poolingformers. Reducing the poolingformer count to zero results in training instability, suggesting that maintaining full-size tokens in the initial layers is crucial. This finding aligns with the observations in Figure 1b: in DiT, the first two attention maps exhibit a uniform distribution, allowing us to replace them with poolingformers, but further replacement disrupts information flow and reduces performance.

**Combination with efficient samplers.** Our FlexDiT is a model compression method that can be seamlessly integrated with efficient samplers, such as DDIM [51] and Rectified Flow (RFlow) [28]. Note that the RFlow variant of DiT was trained by us via 2,000K iterations. As shown in Table 6, when our method is combined with the 25-step DDIM and 5-step Rectified Flow samplers, it achieves approximately 18.7 $\times$  and 93.4 $\times$  improvements in inference speed, respectively, compared to the standard 250-step DDPM. Notably, our method does not introduce a significant performance gap relative to the baseline, demonstrating that it can be effectively combined with efficient samplers.

**The effectiveness of timestep-wise pruning rate.** To evaluate the effectiveness of the timestep-wise pruning rate strategy, we conduct ablation experiments, as shown in Table 7. In these experiments, we maintain the same number of FLOPs while varying the number of tokens along timesteps, either using a constant token count or dynamically adjusting the token count. The results demonstrate that dynamically tuning the pruning rate significantly improves performance. Additionally, Table 7 highlights an observation: the performance of the dynamic pruning strategy is particularly relative with the token count of the later stages of denoising. For instance, the configuration with token counts ranging from 4  $\times$  4 to 8  $\times$  8 only shows a 0.02 FID score increase compared to the configuration with a constant 8  $\times$  8 token count.

## 5. Limitations

The primary limitation of our method arises from the manually pre-defined its structure, containing the number of layers in each module and the number of sparse tokens.

## 6. Conclusion

In this paper, we introduced FlexDiT, a novel method for enhancing the efficiency of DiT by leveraging token sparsity. Through a strategically layered approach that incorporates SDTM and timestep-wise pruning rate, FlexDiT significantly reduces computational complexity while maintaining high generation quality. By decoupling global and local feature extraction with sparse and dense tokens, FlexDiT achieves efficient utilization of resources in both image and video generation tasks. Our experimental results demonstrate substantial reductions in FLOPs with minimal performance degradation, validating FlexDiT’s effectiveness across multiple datasets. Moreover, FlexDiT complements existing methods aimed at optimizing sampling steps, enabling further improvements when used in tandem with enhanced ODE solvers. This work presents a step forward in developing scalable, efficient diffusion models suitable for high-resolution content generation, opening up new possibilities for practical applications of DiT-based architectures.

## References

- [1] Fan Bao, Chongxuan Li, Jun Zhu, and Bo Zhang. Analytic-DPM: an analytic estimate of the optimal reverse variance in diffusion probabilistic models. In *International Conference on Learning Representations*, 2022. 2
- [2] Fan Bao, Shen Nie, Kaiwen Xue, Yue Cao, Chongxuan Li, Hang Su, and Jun Zhu. All are worth words: A vit backbone for diffusion models. In *Proceedings of the IEEE/CVF conference on computer vision and pattern recognition*, pages 22669–22679, 2023. 1
- [3] Andreas Blattmann, Tim Dockhorn, Sumith Kulal, Daniel Mendelevitch, Maciej Kilian, Dominik Lorenz, Yam Levi, Zion English, Vikram Voleti, Adam Letts, et al. Stable video diffusion: Scaling latent video diffusion models to large datasets. *arXiv preprint arXiv:2311.15127*, 2023. 1
- [4] Daniel Bolya and Judy Hoffman. Token merging for fast stable diffusion. *CVPR Workshop on Efficient Deep Learning for Computer Vision*, 2023. 3
- [5] Daniel Bolya, Cheng-Yang Fu, Xiaoliang Dai, Peizhao Zhang, Christoph Feichtenhofer, and Judy Hoffman. Token merging: Your ViT but faster. In *International Conference on Learning Representations*, 2023. 3
- [6] Tim Brooks, Bill Peebles, Connor Holmes, Will DePue, Yufei Guo, Li Jing, David Schnurr, Joe Taylor, Troy Luhman, Eric Luhman, et al. Video generation models as world simulators, 2024. 1
- [7] Shuning Chang, Pichao Wang, Ming Lin, Fan Wang, David Junhao Zhang, Rong Jin, and Mike Zheng Shou. Making vision transformers efficient from a token sparsification view. In *Proceedings of the IEEE/CVF Conference on Computer Vision and Pattern Recognition*, pages 6195–6205, 2023. 3
- [8] Junsong Chen, Jincheng Yu, Chongjian Ge, Lewei Yao, Enze Xie, Yue Wu, Zhongdao Wang, James Kwok, Ping Luo,

Huchuan Lu, and Zhenguo Li. Pixart- $\alpha$ : Fast training of diffusion transformer for photorealistic text-to-image synthesis, 2023. 6, 7

[9] Tianlong Chen, Yu Cheng, Zhe Gan, Lu Yuan, Lei Zhang, and Zhangyang Wang. Chasing sparsity in vision transformers: An end-to-end exploration. *Advances in Neural Information Processing Systems*, 34:19974–19988, 2021. 3

[10] Xinwang Chen, Ning Liu, Yichen Zhu, Feifei Feng, and Jian Tang. Edt: An efficient diffusion transformer framework inspired by human-like sketching. *arXiv preprint arXiv:2410.23788*, 2024. 3

[11] Jia Deng, Wei Dong, Richard Socher, Li-Jia Li, Kai Li, and Li Fei-Fei. Imagenet: A large-scale hierarchical image database. In *2009 IEEE conference on computer vision and pattern recognition*, pages 248–255. Ieee, 2009. 2, 6

[12] Prafulla Dhariwal and Alexander Nichol. Diffusion models beat gans on image synthesis. *Advances in neural information processing systems*, 34:8780–8794, 2021. 1, 6

[13] Patrick Esser, Sumith Kulal, Andreas Blattmann, Rahim Entezari, Jonas Müller, Harry Saini, Yam Levi, Dominik Lorenz, Axel Sauer, Frederic Boesel, et al. Scaling rectified flow transformers for high-resolution image synthesis. In *Forty-first International Conference on Machine Learning*, 2024. 1, 3

[14] Gongfan Fang, Xinyin Ma, and Xinchao Wang. Structural pruning for diffusion models. In *Advances in Neural Information Processing Systems*, 2023. 3

[15] Mohsen Fayyaz, Soroush Abbasi Koohpayegani, Farnoush Rezaei Jafari, Sunando Sengupta, Hamid Reza Vaezi Joze, Eric Sommerlade, Hamed Pirsavash, and Jürgen Gall. Adaptive token sampling for efficient vision transformers. In *European Conference on Computer Vision*, pages 396–414. Springer, 2022. 3

[16] Shanghua Gao, Pan Zhou, Ming-Ming Cheng, and Shuicheng Yan. Mdtv2: Masked diffusion transformer is a strong image synthesizer. *arXiv preprint arXiv:2303.14389*, 2023. 3

[17] Martin Heusel, Hubert Ramsauer, Thomas Unterthiner, Bernhard Nessler, and Sepp Hochreiter. Gans trained by a two time-scale update rule converge to a local nash equilibrium. *Advances in neural information processing systems*, 30, 2017. 2, 6

[18] Jonathan Ho and Tim Salimans. Classifier-free diffusion guidance. *arXiv preprint arXiv:2207.12598*, 2022. 6

[19] Jonathan Ho, Ajay Jain, and Pieter Abbeel. Denoising diffusion probabilistic models. *Advances in neural information processing systems*, 33:6840–6851, 2020. 1, 2

[20] Yi Huang, Jiancheng Huang, Yifan Liu, Mingfu Yan, Jiaxi Lv, Jianzhuang Liu, Wei Xiong, He Zhang, Shifeng Chen, and Liangliang Cao. Diffusion model-based image editing: A survey. *arXiv preprint arXiv:2402.17525*, 2024. 5

[21] Dongjun Kim, Chieh-Hsin Lai, Wei-Hsiang Liao, Naoki Murata, Yuhta Takida, Toshimitsu Uesaka, Yutong He, Yuki Mitsufuji, and Stefano Ermon. Consistency trajectory models: Learning probability flow ODE trajectory of diffusion. In *The Twelfth International Conference on Learning Representations*, 2024. 3

[22] Alexander Kirillov, Eric Mintun, Nikhila Ravi, Hanzi Mao, Chloe Rolland, Laura Gustafson, Tete Xiao, Spencer Whitehead, Alexander C Berg, Wan-Yen Lo, et al. Segment anything. In *Proceedings of the IEEE/CVF International Conference on Computer Vision*, pages 4015–4026, 2023. 7

[23] Tuomas Kynkänniemi, Tero Karras, Samuli Laine, Jaakkko Lehtinen, and Timo Aila. Improved precision and recall metric for assessing generative models. *Advances in neural information processing systems*, 32, 2019. 6

[24] Lijiang Li, Huixia Li, Xiawu Zheng, Jie Wu, Xuefeng Xiao, Rui Wang, Min Zheng, Xin Pan, Fei Chao, and Rongrong Ji. Autodiffusion: Training-free optimization of time steps and architectures for automated diffusion model acceleration. In *Proceedings of the IEEE/CVF International Conference on Computer Vision*, pages 7105–7114, 2023. 3

[25] Xiuyu Li, Yijiang Liu, Long Lian, Huanrui Yang, Zhen Dong, Daniel Kang, Shanghang Zhang, and Kurt Keutzer. Q-diffusion: Quantizing diffusion models. In *Proceedings of the IEEE/CVF International Conference on Computer Vision*, pages 17535–17545, 2023. 3

[26] Yaron Lipman, Ricky TQ Chen, Heli Ben-Hamu, Maximilian Nickel, and Matt Le. Flow matching for generative modeling. *arXiv preprint arXiv:2210.02747*, 2022. 1, 3

[27] Enshu Liu, Xuefei Ning, Zinan Lin, Huazhong Yang, and Yu Wang. OMS-DPM: Optimizing the model schedule for diffusion probabilistic models. In *Proceedings of the 40th International Conference on Machine Learning*, pages 21915–21936. PMLR, 2023. 3

[28] Xingchao Liu, Chengyue Gong, and Qiang Liu. Flow straight and fast: Learning to generate and transfer data with rectified flow. *arXiv preprint arXiv:2209.03003*, 2022. 1, 3, 9

[29] Cheng Lu, Yuhao Zhou, Fan Bao, Jianfei Chen, Chongxuan Li, and Jun Zhu. Dpm-solver: A fast ode solver for diffusion probabilistic model sampling in around 10 steps. *Advances in Neural Information Processing Systems*, 35:5775–5787, 2022. 1, 2

[30] Cheng Lu, Yuhao Zhou, Fan Bao, Jianfei Chen, Chongxuan Li, and Jun Zhu. Dpm-solver++: Fast solver for guided sampling of diffusion probabilistic models. *arXiv preprint arXiv:2211.01095*, 2022. 2

[31] Simian Luo, Yiqin Tan, Longbo Huang, Jian Li, and Hang Zhao. Latent consistency models: Synthesizing high-resolution images with few-step inference, 2023. 1, 3

[32] Xinyin Ma, Gongfan Fang, and Xinchao Wang. Deepcache: Accelerating diffusion models for free. In *Proceedings of the IEEE/CVF Conference on Computer Vision and Pattern Recognition*, pages 15762–15772, 2024. 3

[33] Xin Ma, Yaohui Wang, Gengyun Jia, Xinyuan Chen, Ziwei Liu, Yuan-Fang Li, Cunjian Chen, and Yu Qiao. Latte: Latent diffusion transformer for video generation. *arXiv preprint arXiv:2401.03048*, 2024. 2, 6

[34] Chenlin Meng, Robin Rombach, Ruiqi Gao, Diederik Kingma, Stefano Ermon, Jonathan Ho, and Tim Salimans. On distillation of guided diffusion models. In *Proceedings of the IEEE/CVF Conference on Computer Vision and Pattern Recognition*, pages 14297–14306, 2023. 1, 3

[35] Lingchen Meng, Hengduo Li, Bor-Chun Chen, Shiyi Lan, Zuxuan Wu, Yu-Gang Jiang, and Ser-Nam Lim. Adavit: Adaptive vision transformers for efficient image recognition. In *Proceedings of the IEEE/CVF Conference on Computer Vision and Pattern Recognition*, pages 12309–12318, 2022. 3

[36] Taehong Moon, Moonseok Choi, EungGu Yun, Jongmin Yoon, Gayoung Lee, and Juho Lee. Early exiting for accelerated inference in diffusion models. In *ICML 2023 Workshop on Structured Probabilistic Inference \& Generative Modeling*, 2023. 3

[37] Charlie Nash, Jacob Menick, Sander Dieleman, and Peter W Battaglia. Generating images with sparse representations. *arXiv preprint arXiv:2103.03841*, 2021. 6

[38] Alexander Quinn Nichol and Prafulla Dhariwal. Improved denoising diffusion probabilistic models. In *International conference on machine learning*, pages 8162–8171. PMLR, 2021. 8

[39] Zizheng Pan, Bohan Zhuang, De-An Huang, Weili Nie, Zhiding Yu, Chaowei Xiao, Jianfei Cai, and Anima Anandkumar. T-stitch: Accelerating sampling in pre-trained diffusion models with trajectory stitching. *arXiv preprint arXiv:2402.14167*, 2024. 6

[40] William Peebles and Saining Xie. Scalable diffusion models with transformers. In *Proceedings of the IEEE/CVF International Conference on Computer Vision*, pages 4195–4205, 2023. 1, 6

[41] Ethan Perez, Florian Strub, Harm De Vries, Vincent Dumoulin, and Aaron Courville. Film: Visual reasoning with a general conditioning layer. In *Proceedings of the AAAI conference on artificial intelligence*, 2018. 4

[42] Yifan Pu, Zhuofan Xia, Jiayi Guo, Dongchen Han, Qixiu Li, Duo Li, Yuhui Yuan, Ji Li, Yizeng Han, Shiji Song, et al. Efficient diffusion transformer with step-wise dynamic attention mediators. *arXiv preprint arXiv:2408.05710*, 2024. 3

[43] Robin Rombach, Andreas Blattmann, Dominik Lorenz, Patrick Esser, and Björn Ommer. High-resolution image synthesis with latent diffusion models. In *Proceedings of the IEEE/CVF conference on computer vision and pattern recognition*, pages 10684–10695, 2022. 1, 2

[44] Olaf Ronneberger, Philipp Fischer, and Thomas Brox. U-net: Convolutional networks for biomedical image segmentation. In *Medical image computing and computer-assisted intervention–MICCAI 2015: 18th international conference, Munich, Germany, October 5–9, 2015, proceedings, part III* 18, pages 234–241. Springer, 2015. 2

[45] Andreas Rössler, Davide Cozzolino, Luisa Verdoliva, Christian Riess, Justus Thies, and Matthias Nießner. Faceforensics: A large-scale video dataset for forgery detection in human faces. *arXiv preprint arXiv:1803.09179*, 2018. 2, 7

[46] Tim Salimans and Jonathan Ho. Progressive distillation for fast sampling of diffusion models. *arXiv preprint arXiv:2202.00512*, 2022. 1, 3

[47] Tim Salimans, Ian Goodfellow, Wojciech Zaremba, Vicki Cheung, Alec Radford, and Xi Chen. Improved techniques for training gans. *Advances in neural information processing systems*, 29, 2016. 6

[48] Yuzhang Shang, Zhihang Yuan, Bin Xie, Bingzhe Wu, and Yan Yan. Post-training quantization on diffusion models. In *Proceedings of the IEEE/CVF conference on computer vision and pattern recognition*, pages 1972–1981, 2023. 3

[49] Andy Shih, Suneel Belkhale, Stefano Ermon, Dorsa Sadigh, and Nima Anari. Parallel sampling of diffusion models. *Advances in Neural Information Processing Systems*, 36, 2024. 3

[50] Aliaksandr Siarohin, Stéphane Lathuilière, Sergey Tulyakov, Elisa Ricci, and Nicu Sebe. First order motion model for image animation. *Advances in neural information processing systems*, 32, 2019. 2, 7

[51] Jiaming Song, Chenlin Meng, and Stefano Ermon. Denoising diffusion implicit models. *arXiv preprint arXiv:2010.02502*, 2020. 1, 2, 9

[52] Yang Song and Prafulla Dhariwal. Improved techniques for training consistency models. *arXiv preprint arXiv:2310.14189*, 2023. 3

[53] Yang Song, Prafulla Dhariwal, Mark Chen, and Ilya Sutskever. Consistency models. *arXiv preprint arXiv:2303.01469*, 2023. 1, 3

[54] Khurram Soomro, Amir Roshan Zamir, and Mubarak Shah. A dataset of 101 human action classes from videos in the wild. *Center for Research in Computer Vision*, 2(11):1–7, 2012. 2, 7

[55] Shengkun Tang, Yaqing Wang, Caiwen Ding, Yi Liang, Yao Li, and Dongkuan Xu. Deediff: Dynamic uncertainty-aware early exiting for accelerating diffusion model generation. *arXiv preprint arXiv:2309.17074*, 2023. 3

[56] Zhiwei Tang, Jiasheng Tang, Hao Luo, Fan Wang, and Tsung-Hui Chang. Accelerating parallel sampling of diffusion models. In *Forty-first International Conference on Machine Learning*, 2024. 3

[57] Thomas Unterthiner, Sjoerd Van Steenkiste, Karol Kurach, Raphael Marinier, Marcin Michalski, and Sylvain Gelly. Towards accurate generative models of video: A new metric & challenges. *arXiv preprint arXiv:1812.01717*, 2018. 7

[58] Fu-Yun Wang, Zhaoyang Huang, Alexander William Bergman, Dazhong Shen, Peng Gao, Michael Lingelbach, Keqiang Sun, Weikang Bian, Guanglu Song, Yu Liu, et al. Phased consistency model. *arXiv preprint arXiv:2405.18407*, 2024. 3

[59] Yulin Wang, Rui Huang, Shiji Song, Zeyi Huang, and Gao Huang. Not all images are worth 16x16 words: Dynamic transformers for efficient image recognition. *Advances in neural information processing systems*, 34:11960–11973, 2021. 3

[60] Wei Xiong, Wenhan Luo, Lin Ma, Wei Liu, and Jiebo Luo. Learning to generate time-lapse videos using multi-stage dynamic generative adversarial networks. In *Proceedings of the IEEE Conference on Computer Vision and Pattern Recognition*, pages 2364–2373, 2018. 2, 7

[61] Xingyi Yang, Daquan Zhou, Jiashi Feng, and Xinchao Wang. Diffusion probabilistic model made slim. In *Proceedings of the IEEE/CVF Conference on computer vision and pattern recognition*, pages 22552–22562, 2023. 3

- [62] Zhuoyi Yang, Jiayan Teng, Wendi Zheng, Ming Ding, Shiyu Huang, Jiazheng Xu, Yuanming Yang, Wenyi Hong, Xiaohan Zhang, Guanyu Feng, et al. Cogvideox: Text-to-video diffusion models with an expert transformer. *arXiv preprint arXiv:2408.06072*, 2024. [1](#)
- [63] Tianwei Yin, Michaël Gharbi, Richard Zhang, Eli Shechtman, Fredo Durand, William T Freeman, and Taesung Park. One-step diffusion with distribution matching distillation. In *Proceedings of the IEEE/CVF Conference on Computer Vision and Pattern Recognition*, pages 6613–6623, 2024. [1](#), [3](#)
- [64] Weihao Yu, Mi Luo, Pan Zhou, Chenyang Si, Yichen Zhou, Xinchao Wang, Jiashi Feng, and Shuicheng Yan. Metaformer is actually what you need for vision. In *Proceedings of the IEEE/CVF conference on computer vision and pattern recognition*, pages 10819–10829, 2022. [5](#)
- [65] Wangbo Zhao, Yizeng Han, Jiasheng Tang, Kai Wang, Yibing Song, Gao Huang, Fan Wang, and Yang You. Dynamic diffusion transformer. *arXiv preprint arXiv:2410.03456*, 2024. [3](#)
- [66] Hongkai Zheng, Weili Nie, Arash Vahdat, Kamyar Azizadenesheli, and Anima Anandkumar. Fast sampling of diffusion models via operator learning. In *International conference on machine learning*, pages 42390–42402, PMLR, 2023. [3](#)
- [67] Yixuan Zhu, Wenliang Zhao, Ao Li, Yansong Tang, Jie Zhou, and Jiwen Lu. Flowie: Efficient image enhancement via rectified flow. In *Proceedings of the IEEE/CVF Conference on Computer Vision and Pattern Recognition*, pages 13–22, 2024. [3](#)
- [68] Yuanzhi Zhu, Xingchao Liu, and Qiang Liu. Slimflow: Training smaller one-step diffusion models with rectified flow. In *European Conference on Computer Vision*, pages 342–359. Springer, 2025. [3](#)
- [69] Zhuofan Zong, Kunchang Li, Guanglu Song, Yali Wang, Yu Qiao, Biao Leng, and Yu Liu. Self-slimmed vision transformer. In *European Conference on Computer Vision*, pages 432–448. Springer, 2022. [3](#)

# FlexDiT: Dynamic Token Density Control for Diffusion Transformer

## Supplementary Material

### 7. Captions in Figure 5

Column 1: The image depicts a beach scene with a large body of water, such as a lake or ocean, and a sandy shoreline. The beach is filled with people, including a group of people swimming in the water.

Column 2: The image depicts a beautiful outdoor dining area with a large number of tables and chairs arranged in a row, overlooking a picturesque lake. The tables are covered with white tablecloths, and there are several umbrellas providing shade for the guests. The scene is set in a lush green field, with a large building in the background, possibly a hotel or a restaurant. The tables are arranged in a way that allows for an unobstructed view of the lake, creating a serene and relaxing atmosphere for the diners. The image has a stylish and elegant feel, with the attention to detail in the table arrangement and the choice of location contributing to a memorable dining experience.

Column 3: The image depicts a busy city street at night, with a group of people standing outside a restaurant and a bar. The scene is set in a European city, and the atmosphere is lively and bustling.

Column 4: The image features a vintage-style train, parked on a track surrounded by trees and grass. The train appears to be an old-fashioned steam engine, which is a type of locomotive powered by steam. The train is positioned in a park-like setting, with a tree-lined path nearby. The scene is set in a sunny day, creating a pleasant atmosphere. The image has a nostalgic and historical feel, evoking a sense of the past and the charm of old-time trains.

### 8. Additional visualization

We provide additional visualizations at a resolution of  $512 \times 512$  on FlexDiT-XL from Figure 6 to Figure 17. The class labels, including “arctic wolf”, “volcano”, “cliff drop-off”, “balloon”, “sulphur-crested cockatoo”, “lion”, “otter”, “coral reef”, “macaw”, “red panda”, “husky”, and “panda”, correspond to the same cases presented in DiT. Readers can compare our results with those of DiT. Our samples demonstrate comparable image quality and fidelity. The classifier-free guidance scale is set to 4.0, and all samples shown here are uncurated.



Figure 6. Uncurated  $512 \times 512$  FlexDiT-XL samples.

Classifier-free guidance scale = 4.0

Class label = “arctic wolf” (270)



Figure 7. Uncurated  $512 \times 512$  FlexDiT-XL samples.

Classifier-free guidance scale = 4.0

Class label = “volcano” (980)



Figure 8. Uncurated  $512 \times 512$  FlexDiT-XL samples.  
Classifier-free guidance scale = 4.0  
Class label = “husky” (250)



Figure 9. Uncurated  $512 \times 512$  FlexDiT-XL samples.  
Classifier-free guidance scale = 4.0  
Class label = “sulphur-crested cockatoo” (89)



Figure 10. Uncurated  $512 \times 512$  FlexDiT-XL samples.

Classifier-free guidance scale = 4.0

Class label = “cliff drop-off” (972)



Figure 11. Uncurated  $512 \times 512$  FlexDiT-XL samples.

Classifier-free guidance scale = 4.0

Class label = “balloon” (417)



Figure 12. Uncurated  $512 \times 512$  FlexDiT-XL samples.

Classifier-free guidance scale = 4.0

Class label = “lion” (291)



Figure 13. Uncurated  $512 \times 512$  FlexDiT-XL samples.

Classifier-free guidance scale = 4.0

Class label = “otter” (360)

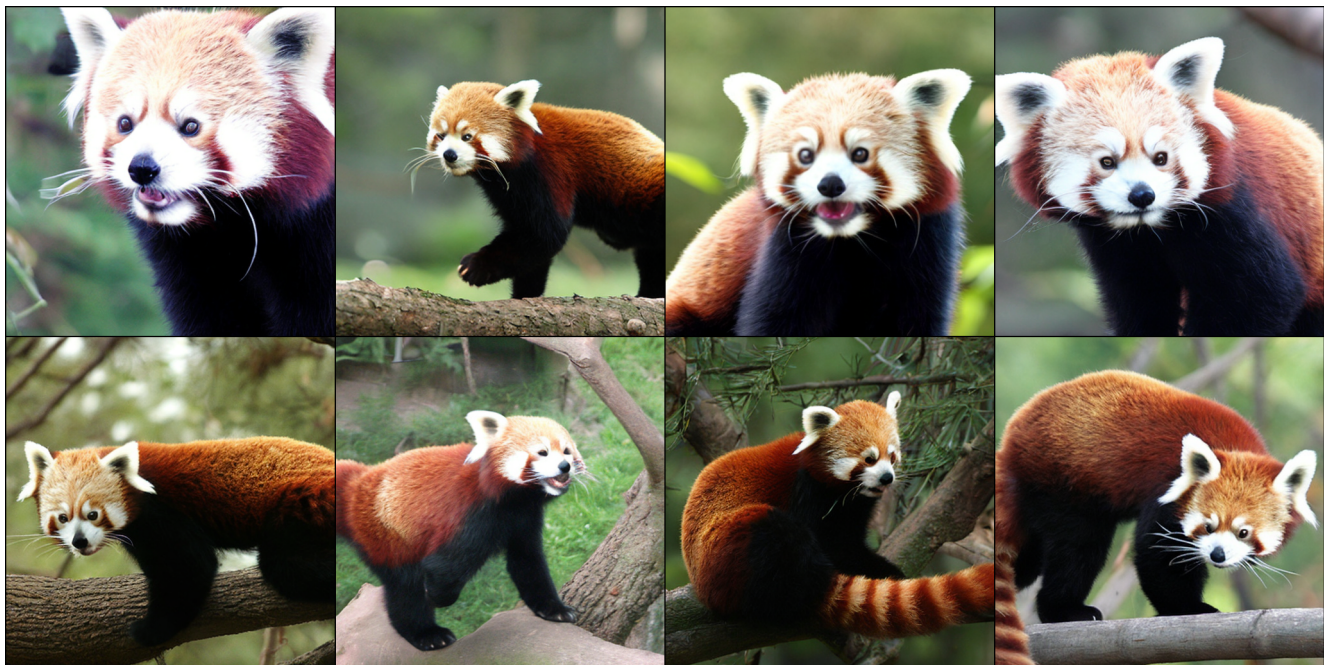


Figure 14. Uncurated  $512 \times 512$  FlexDiT-XL samples.

Classifier-free guidance scale = 4.0

Class label = “red panda” (387)



Figure 15. Uncurated  $512 \times 512$  FlexDiT-XL samples.

Classifier-free guidance scale = 4.0

Class label = “panda” (388)

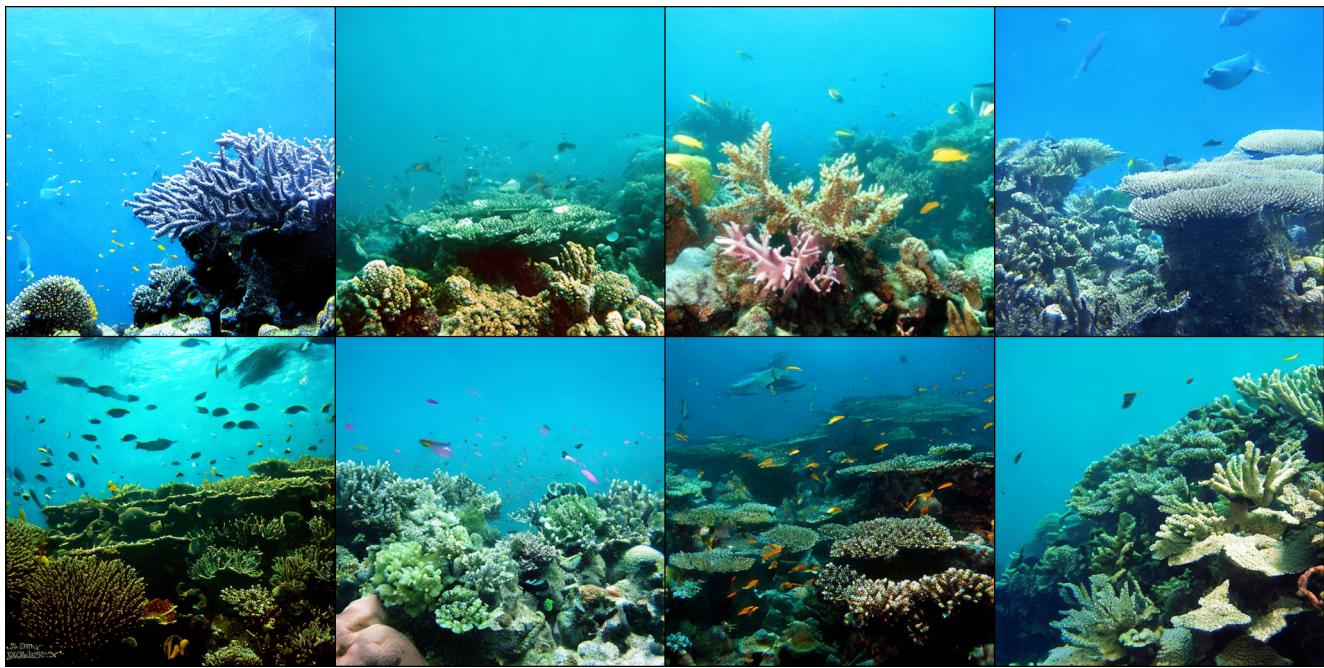


Figure 16. Uncurated  $512 \times 512$  FlexDiT-XL samples.

Classifier-free guidance scale = 4.0

Class label = "coral reef" (973)



Figure 17. Uncurated  $512 \times 512$  FlexDiT-XL samples.

Classifier-free guidance scale = 4.0

Class label = "macaw" (88)